Inorganic Chemistry
Article

Inorg. Chem. **2009**, *48*, 9133–9146 **9133**
DOI: 10.1021/ic9008703

Syntheses, Structures, and Fluorescent Properties of 2-(1H-Imidazol-2-yl)phenols and Their Neutral Zn(II) Complexes

Abiodun Omokehinde Eseola,[†,§] Wen Li,[†] Rong Gao,[‡] Min Zhang,[‡] Xiang Hao,[‡] Tongling Liang,[‡] Nelson Okpako Obi-Egbedi,[§] and Wen-Hua Sun*[,‡]

[†]*Key Laboratory of Photochemical Conversion and Optoelectronic Materials, Technical Institute of Physics and Chemistry, The Chinese Academy of Sciences, Beijing 100190, China,* [‡]*Key Laboratory of Engineering Plastics and Beijing National Laboratory for Molecular Science, Institute of Chemistry, Chinese Academy of Sciences, Beijing, 100190, China, and* [§]*Chemical Sciences Department, Redeemer's University, Redemption City, Ogun, Nigeria*

Received May 5, 2009

A series of 2-(imidazole-2-yl)phenol ligands **L1**−**L6** with the general composition 4-R^4-5-R^3-6-R^2-2-(4,5-R^1,R^1-*1H*-imidazole-2-yl)phenol (**L1**: $R^1 = C_2H_5$, $R^2 = R^3 = R^4 = H$; **L2**: $R^1 = C_6H_5$, $R^2 = R^3 = R^4 = H$; **L3**: $R^1 = C_6H_5$, $R^3 = OCH_3$, $R^2 = R^4 = H$; **L4**: $R^1 = C_6H_5$, $R^4 = OCH_3$, $R^2 = R^3 = H$; **L5**: $R^1 = C_6H_5$, $R^3 = H$, $R^2 = R^4 = CH_3$; **L6**: $R^1 = C_6H_5$, $R^3 = H$, $R^2 = R^4 = t$-Bu) and **L7** (2,4-di-*tert*-butyl-6-(*1H*-phenanthro[9,10-d]imidazol-2-yl)phenol) and their neutral Zn(II) complexes (**Z1**−**Z7**) were synthesized and characterized by spectroscopic and elemental analyses. Molecular structures of **L1**, **L5**, **Z1**, and **Z2** were confirmed by single-crystal X-ray diffraction. **L1** crystallized in the monoclinic *Cc* space group, while **L5**, **Z1**, and **Z2** all crystallized in the triclinic $P\bar{1}$ space group. One-dimensional arrays based on continuous $\pi-\pi$ stacking interactions and hydrogen bonding were observed for **L1** and **Z1**, while **L5** existed as discrete dimeric stack units. **Z2** formed hydrogen-bonded 1D network structures but was completely devoid of $\pi-\pi$ stacking interactions. Emission processes were found to be more dependent on the substituents on phenol as well as condensed media. In contrast to general conclusions on closely related systems in the literature, significant photorelaxation from the excited enol state was observed in the cases of **L1** in methanol and **L4** in both THF and methanol. Therefore, there exists a certain unusual hindering factor to keto−enol phototautomerism in the ligand−solvent systems. The sensing property of zinc(II) complexes was explored regarding the effects of substituents in their ligands. It was observed that coordination to the zinc(II) ion led to emission quenching for **L1** and **L2** while causing an enhancement of fluorescent intensity for **L3**, **L4**, **L5**, and **L6**. A linear relationship was observed between the emission intensity and the concentration of the zinc ion at the 10^{-8} M level. Compared to other zinc compounds in this work, fluorescence enhancement in **Z3** and **Z4** showed that the methoxyl substituent is favorable for fluorescent enhancement.

Introduction

Research efforts on organic or metal-coordinated organic materials with luminescent properties have been of great interest for decades because of their potential applications as electroluminescent components.[1,2] Luminescent materials for light-emitting diodes can be classified into three groups: organic dyes,[3] polymers,[4] or metal complexes.[5] Luminescent materials based on N^O coordination compounds have been extensively investigated since the initial discovery of a bright and stable emission of tris-(8-hydroxyquinolinato)aluminum(III) (Alq3).[5] Luminescent metal complexes have advantages such as the combination of emitting and electron transferring roles, higher environmental stability, and a better extent of diversity that is achievable through tuning of electronic properties by virtue of structural and metal-center variability.[6] Due to the advantages of vacuum-film-forming or thermal deposition properties, zinc complexes chelated by N−O ligands have attracted attention and have proved to be suitable metal−organic precursors of both academic and industrial relevance.[7−9] Through different

*To whom correspondence should be addressed. Tel.: +86 10 62557955. Fax: +86 10 62618239. E-mail: whsun@iccas.ac.cn.

(1) Wang, S. *Coord. Chem. Rev.* **2001**, *215*, 79–98.
(2) Chen, C. H.; Shi, J. *Coord. Chem. Rev.* **1998**, *171*, 161–174.
(3) Adachi, C.; Tsutsui, T.; Saito, S. *Appl. Phys. Lett.* **1990**, *56*, 799–801.
(4) Burroughes, J. H.; Bradly, D. D. C.; Broun, A. R.; Marks, R. N.; Mackay, K.; Friend, R. H.; Burn, P. L.; Holmes, A. B. *Nature*. **1990**, *347*, 539–541.
(5) Tang, C. W.; VanSlyke, S. A. *Appl. Phys. Lett.* **1987**, *51*, 913–915.
(6) Yu, G.; Yin, S.; Liu, Y.; Shuai, Z.; Zhu, D. *J. Am. Chem. Soc.* **2003**, *125*, 14816–14824.
(7) Jang, Y.-K.; Kim, D.-E.; Kim, W.-S.; Kim, B.-S.; Kwon, O.-K.; Lee, B.-J.; Kwon, Y.-S. *Thin Solid Films*. **2007**, *515*, 5075–5078.
(8) Hamada, Y.; Sano, T.; Fujii, H.; Nishio, Y. *Jpn. J. Appl Phys.* **1996**, *35*, L1339–L1341.
(9) Wang, P.; Hong, Z.; Xie, Z.; Tong, S.; Wong, O.; Lee, C.-S.; Wong, N.; Hung, L.; Lee, S. *Chem. Commun.* **2003**, *2003*, 1664–1665.

Published on Web 09/03/2009

Scheme 1. A Summary of the Usual Photocycle of Events Following Excitation of Phenols Bearing Proximal Base (B) Donor Fragments to the Hydroxyl Group

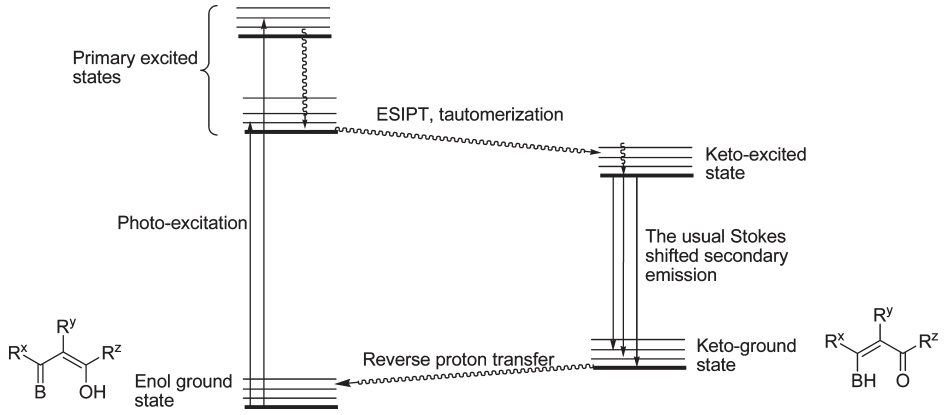

coordination modes, complexes with the same ligands and metal centers can form monomeric or multinuclear structures by virtue of the oxygen acting as a terminal or bridging donor atom, respectively.[6,10] The 2-(imidazol-2-yl)phenol ligand framework is considered a model for the study of Tyr_z-His_{190} cofactor in photosystem II, and its luminescent properties are widely utilized in research studies of biological interest.[11−13]

The introduction of multiple phenyl substituents of chromophores usually improves thermal and amorphous properties in the light-emitting materials as well as affects optical performance by preventing $\pi-\pi$ stacking,[14−16] which is believed to interfere with emission processes.[17] Extension of conjugation by introducing a methoxy group in order to exploit its electron-rich nature has been known to produce an anticipated red shift in electronic spectral bands of organic chromophores.[18]

According to Kasha's rule, fluorescence usually results from the first excited singlet state (S_1) to the ground state (S_0), and the emission spectral shape is usually similar to the corresponding absorption spectra except for the Stokes shift.[19] On photoexcitation, phenols bearing a proximal proton acceptor usually undergo a photoinduced cycle either described as excited state intramolecular proton−electron transfer (ESIPT)[20] or concerted proton−electron transfer,[11,12] which is followed by an enol−keto tautomerism (Scheme 1). ESIPT is reported to be extremely rapid in phenols bearing ortho-substituent fragments.[11] Therefore, phototautomerization in both a solid and solutions of related ligands are normally assigned to relaxation from the respective excited state keto tautomers rather than from the primary excited enol states.[6,9−12,20] Though Zn(II) chelate complexes and others have been extensively explored in search of optimal performance for electroluminescent applications,[6−10] systematic investigations of the optical properties of the ligands and zinc complexes are relatively scarce.[21,22] Therefore, it would be helpful to design new promising fluorophores through a comparative study of optical properties of N^O ligated zinc complexes and the corresponding ligands with an understanding of substituent effects and the influence of condensed media intermolecular interactions. Herein, we present the syntheses, characterization, and photoluminescent properties of 2-(1H-imidazol-2-yl)phenols and their neutral Zn(II) complexes.

Experimental Section

All manipulations of synthesizing organic and complex compounds were performed under a nitrogen atmosphere using standard Schlenk techniques. THF was refluxed and distilled over sodium and benzophenone, while methanol was dried and distilled over CaH_2. All starting materials were obtained commercially as analytical-grade and used without further purification. 2-Hydroxy-3,5-dimethylbenzaldehyde was prepared according to the literature method.[23] All 2-(imidazole-2-yl)phenol derivatives were prepared using a modified literature procedure[24] except for 2,4-di-*tert*-butyl-6-(4,5-diphenyl-*1H*-imidazol-2-yl)phenol (**L6**), which was prepared according to its reported procedure.[25] The synthesized organic compounds were purified on a silica gel column to exclude impurities. Elemental analyses were performed on a Flash EA 1112 microanalyzer. In the cases where there were difficulties of getting satisfactory data for elemental analysis (due to incorporation of the solvent in solid samples), the compounds were dissolved in THF followed by the addition of 5 mL of heptane, evaporation, and vacuum drying for 4 h. ^1H and ^{13}C NMR spectra were recorded on a Bruker ARX-400 MHz instrument using TMS as an internal standard. IR

(10) Tong, Y.-P.; Lin, Y.-W. *J. Chem. Crystallogr*. **2008**, *38*, 613–617.
(11) Markle, T. F.; Rhile, I. J.; DiPasquale, A. G.; Mayer, J. M. *Proc. Natl. Acad. Sci. U. S. A*. **2008**, *105*, 8185–8190.
(12) Rhile, I. J.; Markle, T. F.; Nagao, H.; DiPasquale, A. G.; Lam, O. P.; Lockwood, M. A.; Rotter, K.; Mayer, J. M. *J. Am. Chem. Soc*. **2006**, *128*, 6075–6088.
(13) Lipscomb, W. N.; Strter, N. *Chem. Rev*. **1996**, *96*, 2375–2434.
(14) Satayesh, S.; Grimsdale, A. C.; Weil, T.; Enkelmann, V.; Müllen, K.; Meghdadi, F.; List, E. J. W.; Leising, G. *J. Am. Chem. Soc*. **2001**, *123*, 946–953.
(15) Chen, C.-T.; Chiang, C.-L.; Lin, Y.-C.; Chan, L.-H.; Huang, C.-H.; Tsai, Z.-W.; Chen, C.-T. *Org. Lett*. **2003**, *5*, 1261–1264.
(16) Huang, C.; Zhen, C.-G.; Su, S. P.; Loh, K. P.; Chen, Z.-K. *Org. Lett*. **2005**, *7*, 391–394.
(17) Brinkmann, M.; Gadret, G.; Muccini, M.; Taliani, C.; Masciocchi, N.; Sironi, A. *J. Am. Chem. Soc*. **2000**, *122*, 5147–5157.
(18) Chen, S.; Xu, X.; Liu, Y.; Qiu, W.; Yu, G.; Sun, X.; Zhang, H.; Qi, T.; Lu, K.; Gao, X.; Liu, Y.; Zhu, D. *J. Mater. Chem*. **2007**, *17*, 3788–3795.
(19) Meinardi, F.; Cerminara, M.; Sassella, A.; Borghesi, A.; Spearman, P.; Bongiovanni, G.; Mura, A.; Tubino, R. *Phys. Rev. Lett*. **2002**, *89*, 157403–157406.
(20) Tarkka, R. M.; Zhang, X.; Jenekhe, S. A. *J. Am. Chem. Soc*. **1996**, *118*, 9438–9439.
(21) Tong, Y.-P.; Zheng, S.-L.; Chen, X.-M. *Eur. J. Inorg. Chem*. **2005**, *2005*, 3734–3741.
(22) Sazanovich, I. V.; Kirmaier, C.; Hindin, E.; Yu, L.; Bocian, D. F.; Lindsey, J. S.; Holten, D. *J. Am. Chem. Soc*. **2004**, *126*, 2664–2665.
(23) Wolkenberg, S. E.; Wisnoski, D. D.; Leister, W. H.; Wang, Y.; Zhao, Z.; Lindsley, C. W. *Org. Lett*. **2004**, *6*, 1453–1456.
(24) Eseola, A. O.; Zhang, M.; Xiang, J.-F.; Zuo, W.; Li, Y.; Woods, J. A. O.; Sun, W.-H. *Inorg. Chim. Acta* **2009**, DOI: 10.1016/j.ica.2009.02.026.
(25) Benisvy, L.; Blake, A. J.; Collison, D.; Davies, E. S.; Garner, C. D.; McInnes, E. J. L.; McMaster, J.; Whittaker, G.; Wilson, C. *Chem. Commun*. **2001**, *2001*, 1824–1825.

spectra were recorded on a Nicolet 6700 FT-IR spectrometer as KBr discs in the range of 4000−600 cm^{-1}. The steady-state fluorescent spectra were measured on an F4500-FL fluorescence spectrophotometer; meanwhile, fluorescence lifetimes were obtained using the time-correlated single-photon count technique (Edinburgh Analytical Instruments F900 fluorescence spectrofluorimeter). Thin films of the samples were prepared on quartz slides (1 cm) through spin-coating. Fluorescence quantum yields (Φ_F) were calculated using the comparative method[26,27] using anthracene in ethanol ($\Phi_F = 0.27$) as a standard.

$$\Phi_{F,x} = \Phi_{F,std}\frac{\int I_{F,x}(\nu)\,d\nu}{\int I_{F,std}(\nu)\,d\nu}\left(\frac{1-10^{-A_{std}}}{1-10^{-A_x}}\right)\left(\frac{n_x}{n_{std}}\right)^2$$

$I_{F,x}(\nu)$ and $I_{F,std}(\nu)$ are fluorescence intensities at wavelength ν for the sample and the standard, respectively. A_x and A_{std} are the absorbance at the excitation wavelength for sample x and the standard respectively. n_x and n_{std} are refractive indices of the solvents employed for the sample and standard, respectively.

Preparation of Ligands. 2-(4,5-Diethyl-*1H*-imidazol-2-yl)-phenol (L1). When the modified synthetic procedure of imidazole derivatives was employed,[24] CH_2Cl_2 (20 mL), EtOH (10 mL), catalytic glacial acetic acid (0.5 mL), 3,4-hexanedione (2.2 mL, 17.52 mmol), and salicylaldehyde (1.93 mL, 17.52 mmol) were added via syringe to ammonium acetate (20 g, 0.26 mol) under nitrogen. The reaction mixture was refluxed for 2 h. After cooling and extraction with dichloromethane (100 mL), the combined organic extracts were dried and purified on a silica gel column using dichloromethane/petroleum ether/ethyl acetate (2:6:1) as the eluent to obtain the target compound in two fractions as a free molecule (**L1**, 0.42 g, 11.1%, eluting first) and as an acetic acid adduct (**L1**·CH_3COOH, 0.68 g, 14.0%, eluting second). Analytical data are as follows. **L1**: Mp. 154−155 °C. Selected IR peaks (KBr, cm^{-1}): ν 3256vs, 2964vs, 2930s, 2871m, 1610s, 1588vs, 1490vs, 1388vs, 1261vs, 1134m, 692m. ^{1}H NMR (400 MHz, TMS, $CDCl_3$): δ 7.36 (dd, J = 1.3, 7.8 Hz, 1H); 7.20 (dd, J = 7.1, 8.4 Hz, 1H); 7.20 (d, J = 8.3 Hz, 1H,); 7.03 (d, J = 7.7 Hz, 1H); 6.83(dd, J = 7.3 Hz, 1H); 2.60 (q, J = 7.6 Hz, 4H); 1.25 (t, J = 7.6 Hz, 6H). ^{13}C NMR (100 MHz, TMS, $CDCl_3$): 156.55, 141.73, 131.01, 128.91, 125.97, 118.52, 117.37, 109.76, 17.41, 13.97. Anal. Calcd for $C_{13}H_{16}N_2O$: C, 72.19; H, 7.46; N, 12.95. Found: C, 72.45; H, 7.36; N, 12.90. **L1**·CH_3COOH: Mp. 152−153 °C. Selected IR peaks (KBr, cm^{-1}): ν 3253vs, 2964vs, 2932s, 2873m, 1710vs, 1651s, 1611vs, 1588vs, 1390vs, 1261vs, 1133m, 692m. ^{1}H NMR (400 MHz, TMS, $CDCl_3$): δ 7.42 (d, J = 1.3, 7.8 Hz, 1H); 7.16 (dd, J = 1.5, 7.7 Hz, 1H); 7.00 (d, J = 7.7 Hz, 1H,); 6.79 (dd, J = 7.7 Hz, 1H); 2.59 (q, J = 7.6 Hz, 4H); 2.18 (s, 3H); 1.25 (t, J = 7.6 Hz, 6H). ^{13}C NMR (100 MHz $CDCl_3$, TMS): 177.51, 156.55, 141.73, 131.01, 128.91, 125.97, 118.52, 117.37, 109.76, 31.97, 22.60, 17.41.

2-(4,5-Diphenyl-*1H*-imidazol-2-yl)phenol (L2). To a solution of benzil (2.00 g, 9.51 mmol) and ammonium acetate (14.67 g, 20 equivalent) in refluxing glacial acetic acid (20 mL) was added salicylaldehyde (1.00 mL, 9.51 mmol), and it was refluxed for a further 2 h. The reaction mixture was allowed to cool, transferred to 40 mL of water, carefully neutralized with concentrated aqueous ammonia, and the crude product filtered. After washing with water, the dried solid was recrystallized from ethanol to yield **L2** (2.10 g, 71%). Mp. 200−201 °C. Selected IR peaks (KBr, cm^{-1}): ν 3211s, 3057m, 1601s, 1539m, 1137m, 1071m, 692s. ^{1}H NMR (400 MHz, TMS, $CDCl_3$); δ12.83 (br, s, 1H); 9.37 (br, s, 1H); 7.70−7.50 (br, 4H); 7.49 (d, J = 7.6 Hz, 1H); 7.50−7.30 (br, 6H); 7.32 (dd, J=8.4 Hz, 1H); 7.12 (d, J = 7.6 Hz, 1H); 6.95 (dd, J = 8.4 Hz, 1H). ^{13}C NMR (100 MHz, TMS, $CDCl_3$): 131.35, 130.43, 129.68, 129.01, 128.81, 128.65, 128.03, 127.96, 127.83, 119.69. Anal. Calcd for $C_{21}H_{16}N_2O$: C, 80.75; H, 5.16; N, 8.97. Found: C, 80.66; H, 5.13; N, 8.78.

5-Methoxy-2-(4,5-diphenyl-*1H*-imidazol-2-yl)phenol (L3). In a similar manner as described for **L2**, benzil (1.00 g, 4.76 mmol), 2-hydroxy-4-methoxybenzaldehyde (0.72 g, 4.76 mmol), and ammonium acetate (7.40 g) were treated to obtain white-gray microcrystals of **L3** (1.36 g, 91.4%). Mp. 220−221 °C. Selected IR peaks (KBr, cm^{-1}): ν 3217s, 3060m, 2999w, 1627s, 1602s, 1169m, 1143m, 1076m, 699s. ^{1}H NMR (400 MHz, TMS, $CDCl_3$): δ 12.5−13.5 (s, br, 1H); 9.0−9.2 (s, br, 1H); 7.56 (s, br, 4H); 7.36 (m, br, 7H); 6.63 (d, J = 2.5 Hz, 1H); 6.50 (dd, J = 2.5, 8.6 Hz, 1H); 3.84 (s, 3H). ^{13}C NMR (100 MHz, TMS, $CDCl_3$): 161.74, 159.28, 146.12, 128.72, 127.75, 124.09, 106.59, 105.79, 101.95, 55.37. Anal. Calcd for $C_{22}H_{18}N_2O_2$: C, 77.17; H, 5.30; N, 8.18. Found: C, 77.30; H, 5.36; N, 8.08.

4-Methoxy-2-(4,5-diphenyl-*1H*-imidazol-2-yl)phenol (L4). In a similar reaction procedure as described for **L2**, benzil (0.67 g, 3.21 mmol), 2-hydroxy-5-methoxybenzaldehyde (0.49 g, 3.21 mmol), and ammonium acetate (4.95 g) reacted, and the crude product was purified on a silica gel column with ethylacetate/petroleum ether (1:4). **L4** was obtained as white micro-needles (0.70 g, 64%). Mp. 158−159 °C. Selected IR peaks (KBr, cm^{-1}): ν 3204s, 3059w, 3012w, 2829m, 1602m, 1584m, 1500vs, 762vs. ^{1}H NMR (400 MHz, TMS, $CDCl_3$): δ 7.55 (d, J = 6.9 Hz, 4H); 7.35 (m, 6H); 7.01 (m, 2H); 6.87 (dd, J = 2.9 Hz, 9.0 Hz, 1H); 3.80 (s, 3H). ^{13}C NMR (100 MHz, TMS, $CDCl_3$): 152.28, 151.58, 145.46, 128.73, 128.23, 127.93, 127.83, 118.42, 116.73, 112.34, 108.45, 56.12. Anal. Calcd for $C_{22}H_{18}N_2O_2$: C, 77.17; H, 5.30; N, 8.18. Found: C, 77.01; H, 5.57; N, 8.02.

2,4-Dimethyl-6-(4,5-diphenyl-*1H*-imidazol-2-yl)phenol (L5). In a similar reaction procedure as described for **L2**, benzil (0.35 g, 1.65 mmol), 2-hydroxy-3,5-dimethylbenzaldehyde (0.25 g, 1.65 mmol), and ammonium acetate (2.54 g) were refluxed for 2 h. The products were separated by column chromatography on silica gel (ethyl acetate/petroleum ether, 1:10) to obtain colorless crystals (0.50 g, 90%). Mp. 171−172 °C. Selected IR peaks (KBr, cm^{-1}): ν 3325vs, 3022m, 2952m, 2917s, 1603s, 1587s, 1485vs, 1391s, 1232vs, 1033s, 773vs, 695vs. ^{1}H NMR (400 MHz, TMS, $CDCl_3$): δ 9.25 (s, br, 1H); 7.92 (d, J = 7.8 Hz, 2H); 7.68 (s, br, 2H); 7.47 (dd, J = 7.6 Hz, 4H); 7.39 (M, 4H); 1.57 (s, 6H). $C_{23}H_{20}N_2O$: C, 81.15; H, 5.92; N, 8.23. Found: C, 81.10; H, 5.80; N, 7.88.

2,4-Ditert-butyl-6-(*1H*-phenanthro[9,10-d]imidazol-2-yl)phenol (L7). In a similar reaction procedure as described for **L2**, phenanthrenequinone (2.00 g, 9.61 mmol), ammonium acetate (15.00 g), and 3,5-di-*tert*-butyl-2-hydroxybenzaldehyde (2.25 g, 9.61 mmol) were refluxed for 2 h and purified on a silica gel column with dichloromethane/petroleum ether (1:20) to obtain **L7** (0.60 g, 14.8%). Mp. (dec.) >320 °C. Selected IR peaks (KBr, cm^{-1}): ν 3481s, 3053m, 2949vs, 2906s, 2863s, 1616s, 1543m, 1510m, 1469vs, 1442vs, 1243s, 747vs. ^{1}H NMR (400 MHz, TMS, $CDCl_3$): δ 13.48 (s, 1H); 9.92 (s, 1H); 8.77 (d, J = 8.1 Hz, 1H); 8.69 (dd, J = 8.2 Hz, 2H); 8.13 (d, J = 7.7 Hz, 1H); 7.72 (m, 2H); 7.66 (m, 2H); 7.51 (s, 1H); 7.47 (s, 1H). Anal. Calcd for $C_{29}H_{30}N_2O$: C, 82.43; H, 7.16; N, 6.63. Found: C, 82.32; H, 7.10; N, 6.53.

Preparation of Complexes. Bis(2-(4,5-diethyl-1H-imidazol-2-yl)phenoxy)zinc (Z1). A solution of 2-(4,5-diethyl-1H-imidazol-2-yl)phenol (**L1**; 0.11 g, 0.51 mmol) was made in dichloromethane (2 mL), and zinc acetate dihydrate (56.00 mg, 0.25 mmol) in ethanol (2 mL) was layered over the dichloromethane solution. The reaction system was covered and kept standing for two weeks; complex **Z1** was obtained as colorless crystals (80.00 mg, 29%). Mp./dec 330−332 °C. Selected IR peaks (KBr, cm^{-1}): ν 3170m, 3116, 3028m, 2967s, 1622s, 1557s, 1481vs, 1305vs, 1254vs, 1140vs, 760. Anal. Calcd for $C_{26}H_{30}N_4O_2Zn$: C, 62.97; H, 6.10; N, 11.30. Found: C, 62.82; H, 6.02; N, 11.17.

(26) Hrdlovič, P.; Kollár, J.; Chmela, S. *J. Photochem. Photobiol. A: Chem.* **2004**, *163*, 289–296.
(27) Dawson, W. R.; Windsor, M. W. *J. Phys. Chem.* **1968**, *72*, 3251–3260.

Bis(2-(4,5-diphenyl-*1H*-imidazol-2-yl)phenoxy)zinc (Z2). 2-(4,5-Diphenyl-1H-imidazol-2-yl)phenol (**L2**; 0.26 g, 0.83 mmol) and zinc acetate dihydrate (0.09 g, 0.42 mmol) were dissolved in 20 mL of ethanol and refluxed at 70 °C for 3 h. The resulting precipitate was filtered, washed with a few milliliters of ethanol, and dried to obtain **Z2** as white microcrystals (0.26 g, 88%). Mp./dec 336−338 °C. Selected IR peaks (KBr, cm^{-1}): ν 3621s, 3053m, 1602s, 1554m 1532m, 1305vs, 1246s, 696vs. Anal. Calcd for $C_{42}H_{30}N_4O_2Zn$: C, 73.31; H, 4.39; N, 8.14. Found: C, 73.13; H, 4.41; N, 7.98.

Bis(5-methoxy-2-(4,5-diphenyl-*1H*-imidazol-2-yl)phenoxy)zinc (Z3). 5-Methoxy-2-(4,5-diphenyl-1H-imidazol-2-yl)phenol (**L3**; 0.30 g, 0.88 mmol) and zinc acetate dehydrate (0.10 g, 0.44 mmol) were dissolved in 20 mL of ethanol and stirred at room temperature to produce **Z3** as a white powder (0.24 g, 73%). Mp./dec 356−358 °C. Selected IR peaks (KBr, cm^{-1}): ν 1606vs, 1533m, 1538m, 1490s, 1442s, 1335m, 1209vs, 1144s, 697vs Anal. Calcd for $C_{44}H_{34}N_4O_4Zn$: C, 70.64; H, 4.58; N, 7.49. Found: C, 70.57; H, 4.71; N, 7.56.

Bis(4-methoxy-2-(4,5-diphenyl-*1H*-imidazol-2-yl)phenoxy)zinc (Z4). In the same manner as for **Z2**, 4-methoxy-2-(4,5-diphenyl-1H-imidazol-2-yl)phenol (0.36 g, 1.06 mmol) was reacted with zinc acetate dihydrate (0.12 g, 0.53 mmol) to obtain **Z4** as a white powder (0.32 g, 70.7%). Mp./dec 310−312 °C. Selected IR peaks (KBr, cm^{-1}): ν 3627m, 3053m, 2951m, 2835m, 1591s, 1568s, 1493vs, 1229vs, 1136s, 1042s, 697s. Anal. Calcd for $C_{44}H_{34}N_4O_4Zn$: C, 70.64; H, 4.58; N, 7.49. Found: C, 70.73; H, 4.85; N, 7.34.

Bis(2,4-dimethyl-6-(4,5-diphenyl-*1H*-imidazol-2-yl)phenoxy)zinc (Z5). In a similar manner as for **Z1**, 2,4-dimethyl-6-(4,5-diphenyl-1H-imidazol-2-yl)phenol (**L5**; 0.13 g, 0.39 mmol) was reacted with zinc acetate dihydrate (42.00 mg, 0.19 mmol) to obtain microcrystalline solids of **Z5** (0.50 g, 90%). Mp./dec 302−304 °C. Selected IR peaks (KBr, cm^{-1}): ν 3223br,s, 3054m, 2965m, 2916m, 2859w, 1613s, 1590s, 1476vvs, 1247vs, 1049s, 734vs, 696vs. Anal. Calcd for $C_{46}H_{38}N_4O_2Zn$: C, 74.24; H, 5.15; N, 7.53. Found: C, 74.20; H, 5.42; N, 7.42.

Bis(2,4-di-*tert*-butyl-6-(4,5-diphenyl-*1H*-imidazol-2-yl)phenoxy)zinc (Z6). 2,4-Di-*tert*-butyl-6-(4,5-diphenyl-1H-imidazol-2-yl)phenol (**L6**; 0.21 g, 0.50 mmol) in THF (2 mL) and zinc acetate dihydrate (54.91 mg, 0.25 mmol) in ethanol (5 mL) were mixed and refluxed for 1 h in the presence of triethylamine (1.4 mL). On cooling, the precipitate was filtered and washed with a little ethanol and then dried to afford **Z6** as yellowish microcrystals (64.70 mg, 27%). Mp. 319−320 °C. Selected IR peaks (KBr, cm^{-1}): ν 3660m, 3476m, 3200br,s, 3052m, 2949vs, 2902s, 2865s, 1607s, 1590m, 1527vs, 1326s, 1259vs, 1145s, 773vs, 694vs. Anal. Calcd for $C_{58}H_{62}N_4O_6Zn$: C, 76.34; H, 6.85; N, 6.14. Found: C, 76.20; H, 6.97; N, 6.58.

Bis(2,4-di-*tert*-butyl-6-(*1H*-phenanthro[9,10-d]imidazol-2-yl)phenoxy)zinc (Z7). In a similar manner as for **Z6**, 2,4-di-*tert*-butyl-6-(1H-phenanthro[9,10-d]imidazol-2-yl)phenol (**L7**; 0.20 g, 0.47 mmol) was reacted with zinc acetate dihydrate (52.00 mg, 0.24 mmol) to form **Z7** as yellowish microcrystals (50.30 mg, 21%). Dec. 408−410 °C. Selected IR peaks (KBr, cm^{-1}): ν 3054m, 2955vs, 2907s, 2868s, 1574vvs, 1471vvs, 1399vvs, 1330s, 1260s, 1023s, 755s. Anal. Calcd for $C_{58}H_{58}N_4O_2Zn$: C, 76.68; H, 6.43; N, 6.17. Found: C, 76.91; H, 6.54; N, 6.02.

X-Ray Measurements. Single crystals of **L1** and **L5** were obtained by slow evaporation of their ethanol and dichloromethane solutions, respectively. Single crystals of complex **Z1** were obtained during its synthesis by layering an ethanol solution of zinc acetate over the dichloromethane solution of **L1**. Slow evaporation of the solvent from a methanol solution of **Z2** yielded suitable single crystals. Suitable crystals of compounds **L1**, **L5**, and **Z2** were mounted on a Rigaku R-AXIS Rapid diffractometer, while compound **Z1** was mounted on a Rigaku Saturn 724 diffractometer. Both diffractometers employ graphite-monochromated Mo Kα radiation and operated at −100 °C. Cell parameters were obtained by global refinement of the positions of all collected reflections. Intensities were corrected for Lorentz and polarization effects and empirical (**Z2**, **L1**, and **L5**) or numerical (**Z1**) absorptions. The structures were solved by direct methods and refined by full-matrix least squares on F^2. All non-hydrogen atoms were refined anisotropically, and all hydrogen atoms were placed in calculated positions. Structure solution and refinement were performed using the SHELX-97 package.[28] Crystallographic data of compounds **L1**, **L5**, **Z1**, and **Z2** are summarized in Table 1.

Results and Discussion

Synthesis of Ligands. 2-Hydroxy-3,5-dimethylbenzaldehyde[23] and the imidazolyl ligands[24,25] were prepared by modified procedures of reported methods. A condensation reaction of α-dicarbonyls and aldehydes was conducted in the presence of excess ammonium acetate as the source of the imidazole nitrogen atoms. In order to alter the electronic environments of the five-membered imidazole and six-membered phenol rings of the 2-(1H-imidazol-2-yl)phenol nucleus, a rational reaction of appropriate salicylaldehyde derivatives with selected α-dicarbonyls was considered for the preparation of **L1**−**L7**. A general synthetic sketch of the ligands is presented in Scheme 2.

During condensation of 3,4-hexandione and salicylaldehyde in attempts to prepare 2-(4,5-diethyl-*1H*-imidazol-2-yl)phenol (**L1**), employing glacial acetic acid as a catalytic reagent as well as a reaction medium was found to be unfavorable. This is probably due to the fate suffered by the dicarbonyl in the presence of such a large amount of acetic acid. Employing ethanol/dichloromethane (1:1) as a reaction medium in the presence of a catalytic amount of glacial acetic acid (0.5 mL) afforded **L1** in acceptable yields (total 25%) as a free ligand (**L1**) and an acetic acid adduct (**L1**·CH_3COOH). There were signals at δ 2.18(s, 3H) ppm, 177.5 ppm, and 1710 cm^{-1} respectively in the ^1H NMR, ^{13}C NMR, and IR spectra assigned to the acetic acid fragment of **L1**·CH_3COOH. A similar observation was previously reported.[29] In the preparation of 2,4-di-*tert*-butyl-6-(*1H*-phenanthro[9,10-d]imidazol-2-yl)phenol (**L7**), a relatively low yield (15%) was recorded for the reaction of phenanthrenequinone with 3,5-di-*tert*-butyl-2-hydroxybenzaldehyde, and this is due to the competing formation of the oxazole analogue, which was typically isolated in greater yields than the target imidazole ligand. All organic compounds were characterized by NMR, IR, and elemental analysis. Melting point analysis revealed a rather high melting point/decomposition temperature value for **L7** (>320) and probably suggests the existence of a zwitterionic form in the solid state.

Synthesis of Complexes. Neutral zinc complexes containing two ligands are generally recognized as potentially important candidates for the preparation of excellent electroluminescent materials.[1,2,6,7,21] The challenge associated with obtaining suitable single crystals for bidentate zinc complexes was recently discussed[21,30] and has necessitated

(28) Sheldrick, G. M. *SHELXL-97*; University of Göttingen: Göttingen, Germany, 1997.
(29) Wen, H.-L.; He, M.; Liu, C.-B. *Acta Crystallogr.* **2008**, *E64*, o1949–o1949.
(30) Tong, Y.-P.; Zheng, S.-L.; Chen, X.-M. *Inorg. Chem.* **2005**, *44*, 4270–4275.

Table 1. Crystal Data and Processing Parameters for **L1**, **L5**, **Z1**, and **Z2**

	L1	**L5**·CH_3CH_2OH	**Z1**·CH_3CH_2OH	**Z2**·$3CH_3OH$
formula	$C_{13}H_{16}N_2O$	$C_{23}H_{20}N_2O \cdot C_2H_6O$	$C_{26}H_{30}N_4O_2Zn \cdot C_2H_6O$	$C_{42}H_{30}N_4O_2Zn \cdot C_3H_{12}O_3$
fw	216.28	386.48	495.91	784.22
temp (K)	173(2)	173(2)	173(2)	173(2)
wavelength (Å)	0.71073	0.71073	0.710747	0.71073
cryst syst	monoclinic	triclinic	triclinic	triclinic
space group	*Cc*	$P\bar{1}$	$P\bar{1}$	$P\bar{1}$
a (Å)	13.748(3)	8.2745(2)	11.207(2)	12.401(3)
b (Å)	20.316(4)	11.232(2)	11.295(2)	12.590(3)
c (Å)	13.030(3)	12.311(3)	12.353(3)	14.729(3)
α (deg)	90.00(0)	73.11(3)	101.06(3)	67.34(3)
β (deg)	99.34(3)	73.80(3)	110.62(3)	67.89(3)
γ (deg)	90.00(0)	88.26(3)	102.46(3)	75.34(3)
volume ($Å^3$)	3591.4(12)	1049.7(4)	1366.2(5)	1950.3(8)
Z	12	2	2	2
calcd density ($g \cdot m^{-3}$)	1.200	1.223	1.206	1.335
μ (mm^{-1})	0.077	0.078	0.685	0.681
F(000)	1392	412	784	820
cryst size (mm)	0.90 × 0.35 × 0.15	0.70 × 0.40 × 0.26	0.35 × 0.14 × 0.13	0.58 × 0.57 × 0.39
θ range (deg)	1.81−27.48	1.80−27.48	1.93−27.49	1.95−25.00
limiting indices	$-17 \le h \le +17$	$-10 \le h \le +10$	$-14 \le h \le +14$	$-12 \le h \le +12$
	$-23 \le k \le +26$	$-14 \le k \le +14$	$-14 \le k \le +14$	$-11 \le k \le +11$
	$-16 \le l \le +16$	$-15 \le l \le +15$	$-16 \le l \le +16$	$-26 \le l \le +26$
no. of rflns collected	7181	8674	16816	12723
no. of unique rflns	7181	4798	6209	6853
R(int)	0.0422	0.0313	0.0367	0.0286
completeness (%) to θ (^{deg})	99.8, θ = 27.48	99.6, θ = 27.48	98.8, θ = 27.49	99.69, θ = 25.00
no. of params	447	277	298	511
goodness-of-fit on F^2	1.059	1.281	1.122	1.106
final R indices ($I > 2\sigma(I)$)	R1 = 0.0720	R1 = 0.0734	R1 = 0.0566	R1 = 0.0431
	wR2 = 0.1373	wR2 = 0.1697	wR2 = 0.1665	wR2 = 0.0917
R indices (all data)	R1 = 0.1165	R1 = 0.0983	R1 = 0.0636	R1 = 0.0550
	wR2 = 0.1517	wR2 = 0.1876	wR2 = 0.1739	wR2 = 0.0957
largest diff. peak and hole (e $Å^{-3}$)	0.483, −0.628	0.281, −0.518	0.514, −0.823	0.302, −0.378

Scheme 2. Synthesis of Ligands **L1**−**L7**

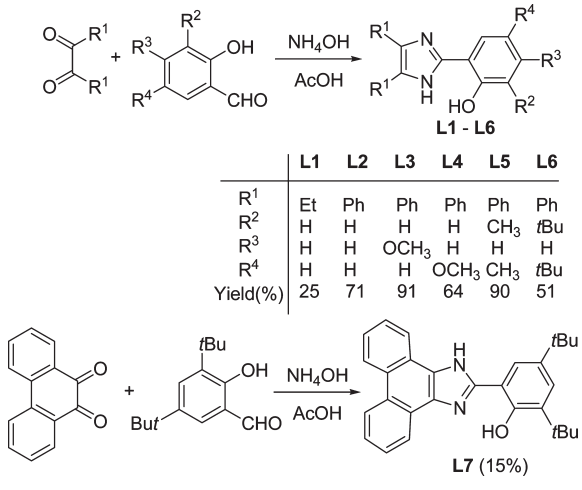

	L1	L2	L3	L4	L5	L6
R^1	Et	Ph	Ph	Ph	Ph	Ph
R^2	H	H	H	H	CH_3	*t*Bu
R^3	H	H	OCH_3	H	H	H
R^4	H	H	H	OCH_3	CH_3	*t*Bu
Yield(%)	25	71	91	64	90	51

Scheme 3. Synthesis of the Zinc Complexes

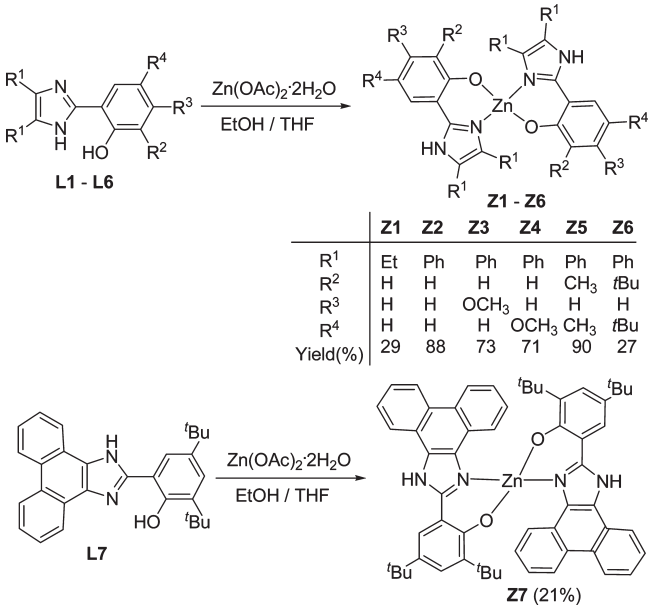

	Z1	Z2	Z3	Z4	Z5	Z6
R^1	Et	Ph	Ph	Ph	Ph	Ph
R^2	H	H	H	H	CH_3	*t*Bu
R^3	H	H	OCH_3	H	H	H
R^4	H	H	H	OCH_3	CH_3	*t*Bu
Yield(%)	29	88	73	71	90	27

attempts through high-vacuum sublimation of the powder complexes,[6] hydrothermal methods of complex preparation, solvent diffusion or evaporation, and so forth. However, it may not pose such a difficulty to obtain the zinc complex crystals. After obtaining the above imidazolyl−phenol derivatives (**L1**−**L7**), their zinc complexes were easily formed through the direct reactions of such imidazolyl−phenol derivatives with zinc salt in solutions (Scheme 3).

Due to the different substituents, however, the ligands exhibited various reactivities toward the zinc salt. The ligands with an unsubstituted phenol ring (**L1** and **L2**) are capable of forming the respective complexes (**Z1** and **Z2**) by mixing in ethanol at room temperature. The ligands (**L3** and **L4**) bearing an electron-donating methoxyl substituent exhibited faster precipitation of the complexes (**Z3** and **Z4**), in which the formation of **Z4** was faster than that of **Z3** because of the stronger influence of the para-substituent in **L4** than that of the meta-substituent in **L3**. With a bulky substituent of the *tert*-butyl group, ligands **L6** and **L7** were most reluctant in the chelation and required the addition of base to aid the reaction.

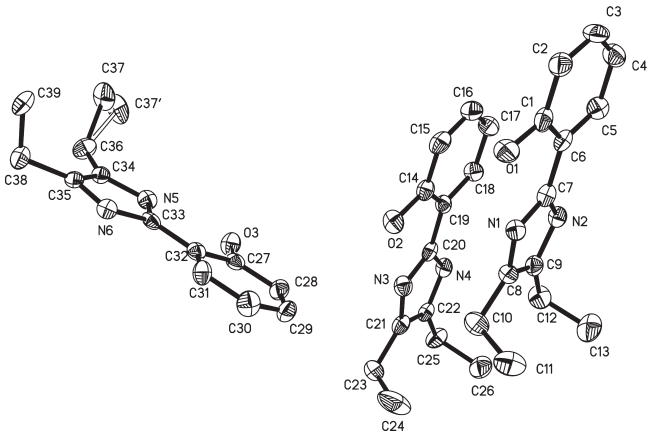

Figure 1. Molecular structures of **L1** showing three crystallographically independent units with thermal ellipsoids drawn at the 50% probability level. Some hydrogen atoms and labels have been omitted for clarity, and C37 is disordered.

All complexes were characterized by elemental analysis and IR spectroscopy. The vibrations of active phenolic protons of the ligands were absent in their complexes, and IR peaks around the 1600 cm^{-1} region were shifted to lower wavenumbers in the zinc complexes (e.g., 1622 cm^{-1} and 1600 cm^{-1} for **L1** compared to 1610 cm^{-1} and 1588 cm^{-1} for **Z1**; 1590 cm^{-1} for **L5** compared 1568 cm^{-1} for **Z5**; and 1615 cm^{-1} for **L7** compared to 1587 cm^{-1} for **Z7**). These are evidence indicating the coordination of ligand with the zinc center. These zinc complexes likely decomposed before melting, but **Z6** exhibited melting into light yellow oil without apparent signs of decomposition. Moreover, the molecular structures of representative ligands (**L1** and **L5**) and complexes (**Z1** and **Z2**) were confirmed by single-crystal X-ray diffraction.

Structures. The molecular structures of **L1** and **L5** in the solid state were determined by X-ray diffraction, and both compounds clearly showed interactions between molecules. Meanwhile, the compound **L5** crystallized along with an ethanol solvate. **L1** crystallized in the monoclinic *Cc* space group and revealed three independent molecules per unit cell (Figure 1), in which C37 is disordered. The phenol and imidazolyl rings are almost coplanar with each other, with dihedral angles in the range of 3.36−4.72°. The bond lengths, angles, and hydrogen-bond parameters are provided in the Supporting Information.

In the solid of **L1**, the phenol ring of one molecule interacts in an "offset face-to-face" fashion with another imidazolyl ring of a contiguous moiety (Figure 2), and the interplanar distance is 3.306 Å as a $\pi-\pi$ interaction. The intramolecular and intermolecular hydrogen bonds (Table 2) furnished a 1D array of the ligand molecules, which is similar to the observation of arrangement in 2-(2-hydroxyphenyl)benzimidazole and 5-amino-2-(1H-benzoimidazol-2-yl)phenol.[21]

Unlike for **L1**, **L5** crystallized with incorporating ethanol molecules in the triclinic $P\bar{1}$ space group (Figure 3), in which C25 is disordered. The dihedral angle of the phenol ring with imidazolyl ring is 5.86°, which is notably larger than that of **L1** (3.36−4.72°). Structural differences are caused by steric effects of ethyl and phenyl substituents on

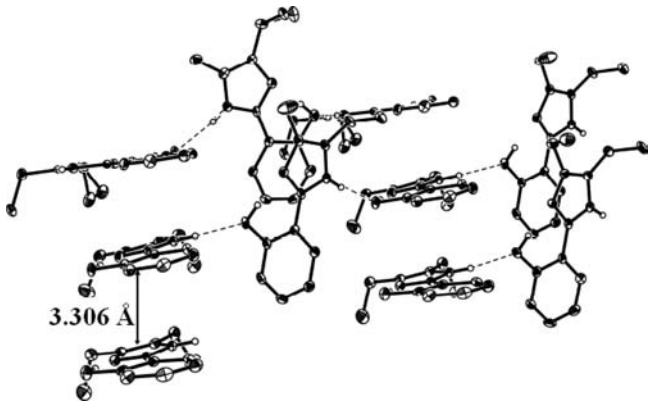

Figure 2. 1D-linkage hydrogen-bonding interactions in **L1**.

the imidazole ring. The steric bulk of the two phenyl rings in **L5** would be effective in contributing to the reduced coplanarity between the imidazolyl and phenol rings. The bond lengths, angles, and hydrogen-bond parameters are provided in the Supporting Information.

In the solid of **L5**, there exist discrete dimeric $\pi-\pi$ stackings locked on either side by hydrogen bonds involving solvent molecules (Figure 4, Table 3). As observed for **L1**, the phenol ring of one molecule interacts in an "offset face-to-face" fashion with the imidazolyl ring of the partner molecule in the dimeric unit of **L5** with an interplanar separation of 3.484 Å. In addition, the intramolecular and intermolecular hydrogen bonds between molecules of **L5** and ethanol solvate involved in pairing interaction are within expected values (Table 3).

The molecular structure of complex **Z1** incorporated with one ethanol molecule is shown in Figure 5, and its selected bond lengths and angles are reported in Table 4. Though the geometry at each zinc center can be best described as a distorted tetrahedron in which two chelating ligands are placed in a similar disposition about the metal center, slight differences still occur: a longer Zn(1)−O(1) bond length of 1.946(2) Å and smaller dihedral angle (C(1)−C(6)−C(7)−N(1)) of 1.00° were observed for one ligand, while the respective values for the second ligand are 1.918 Å for Zn(1)−O(2) and 7.49° for C(14)−C(19)−C(20)−N(3). These dihedral angles represent a relative twist in the phenolate−imidazole ring planes about the C−C bond joining the rings.

In the packing pattern observed for complex **Z1** (Figure 6), the $\pi-\pi$ stacking interaction (alternating face-to-face distances of 3.396 Å and 3.501 Å) assisted by solvent-mediated hydrogen bonding (Table 5) held each complex unit to the left and right neighboring units along a 1D array. The ethanol lattice solvent in **Z1** is disordered and was squeezed[31,32] before writing the final structure refinement files. The average location of the solvent is $x = 0.500$, $y = 0.000$, and $z = 1.000$, and its volume is 224 $Å^{-3}$ with 96 electrons contained.

As encountered for **Z1**, complex **Z2** also bears a distorted tetrahedral geometry about the zinc center (Figure 7). The basal plane is composed of O1, N1, and N3, and the zinc atom deviates from the basal plane by 0.496 Å. The dihedral angles between the coordination

(31) Spek, A. L. *J. Appl. Crystallogr.* **2003**, *36*, 7–13.
(32) Vandersluis, P.; Spek, A. L. *Acta Crystallogr.* **1990**, *A46*, 194–201.

Table 2. Hydrogen Bond Parameters for **L1**[a]

	D−H (Å)	D−H···A (deg)	D···A (Å)	H···A (Å)
O(1)−H(1)···N(1)	0.840	149.09	2.581	1.824
O(2)−H(2)···N(3)	0.840	149.69	2.589	1.835
O(3)−H(3)···N(5)	0.840	149.43	2.589	1.830
N(2)−H(2A)···O(1)#1	0.880	171.34	2.894	2.020
N(4)−H(4A)···O(2)#1	0.880	172.54	2.899	2.024
N(6)−H(6A)···O(3)#2	0.880	172.38	2.906	2.032

[a] Symmetry transformations used to generate equivalent atoms: (#1) $x, -y, z + 1/2$; (#2) $x, -y, z - 1/2$.

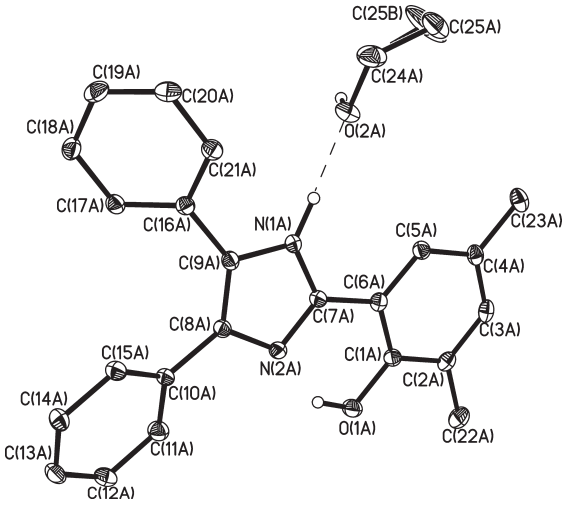

Figure 3. Ortep plot of **L5**·CH_3CH_2OH with thermal ellipsoids drawn at the 50% probability level. Some hydrogen atoms have been omitted for clarity, and C(25) of the ethanol molecule is disordered.

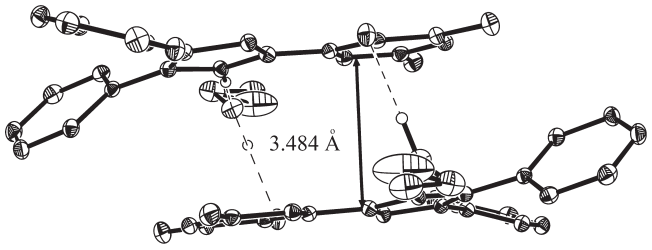

Figure 4. Discrete $\pi-\pi$ stacking interactions observed in the crystal pack of **L5**·CH_3CH_2OH.

Table 3. Hydrogen Bond Parameters for **L5**·CH_3CH_2OH

	D−H (Å)	D−H···A (deg)	D···A (Å)	H···A (Å)
O(1)−H(1O)···N(2)	0.903	146.39	2.584	1.783
O(2)−H(2O)···O(1)	0.961	161.14	2.878	1.952
N(1)−H(2N)···O(2)	1.000	177.04	2.868	1.869

ring atoms on the phenol and imidazole rings of the two chelated ligands are significantly larger (15.82 and 21.52°) than those observed for **Z1** (1.00 and 7.49°). Moreover, one coordination plane (N(1)−O(1)−Zn(1)) in **Z2** is approximately perpendicular to the other (N(3)−O(2)−Zn(1)) with a dihedral angle of 89.38°, which is bigger than the corresponding value for **Z1** (84.00°). The significant differences observed are considered to result from the steric effects between the small ethyl and the bulky phenyl substituents. Metal−ligand bond lengths

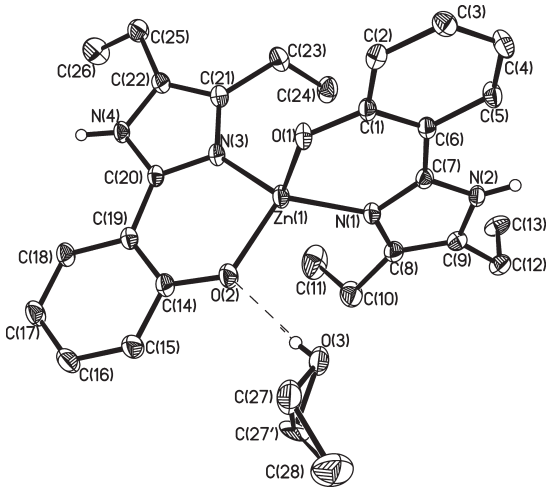

Figure 5. Ortep plot of **Z1**·C_2H_5OH with thermal ellipsoids drawn at the 50% probability level. Hydrogen atoms linked on carbon atoms have been omitted for clarity.

Table 4. Selected Bond Lengths (Å) and Angles (Degree) for **Z1**·CH_3CH_2OH and **Z2**·$3CH_3OH$

	Z1·CH_3CH_2OH	**Z2**·$3CH_3OH$
	Bond Lengths	
Zn(1)−O(2)	1.918(2)	1.9383(19)
Zn(1)−O(1)	1.946(2)	1.9392(17)
Zn(1)−N(1)	1.953(3)	1.978(2)
Zn(1)−N(3)	1.959(2)	1.965(2)
	Bond Angles	
O(2)−Zn(1)−O(1)	116.33(10)	109.69(8)
O(2)−Zn(1)−N(1)	115.12(10)	110.42(8)
O(1)−Zn(1)−N(1)	96.13(10)	95.05(8)
O(2)−Zn(1)−N(3)	96.61(10)	96.10(8)
O(1)−Zn(1)−N(3)	109.94(10)	121.09(8)
N(1)−Zn(1)−N(3)	124.00(11)	124.51(8)

and angles for **Z1** and **Z2** are in the range of values reported for other zinc N−O systems.[6,10]

In the packing pattern observed for **Z2** (Figure 8), each complex unit interacts with another through hydrogen bonding via incorporated solvent molecules and forms a 1D array (Table 6).

Absorption Properties. The absorption spectra of all organic ligands and complexes were recorded under the same instrument settings and at room temperature (about 23 °C). All ligands exhibit the wavelength absorption peaks around 320 nm in their solutions (5×10^{-5} M) of tetrahydrofuran (THF), methanol, or dimethylformamide (DMF), which can be considered to be absorptions belonging to $\pi-\pi^*$ transitions on the basis of extinction

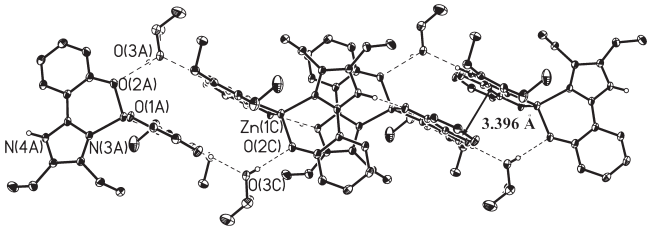

Figure 6. Continuous 1D-array in **Z1**·C_2H_5OH achieved by $\pi-\pi$ stacking and ethanol mediated H-bonding.

Table 5. Hydrogen Bond Parameters for **Z1**·CH_3CH_2OH

	D−H (Å)	D−H···A (deg)	D···A (Å)	H···A (Å)
N(4)−H(4A)···O(1)	0.880	140.08	2.788	2.056
C(5)−H(5)···N(2)	0.950	101.68	2.883	2.537
C(18)−H(18)···N(4)	0.950	101.82	2.886	2.538

coefficients ($\varepsilon_{\lambda max}$, Table 7). The solvents are selected on the basis of their varying dielectric constants (THF, 7.5; MeOH, 33; DMF, 38) and protic/aprotic natures. In general, absorption peaks were slightly blue-shifted in methanol compared to those in THF. When the absorption positions of ligands in THF and DMF were compared, the peaks hardly showed a response to solvent polarities (i.e., 0 − 2 nm shifts), except for **L1**, with a shift of 13 nm. Polarities of the solvents might not be important in affecting electronic properties of the compounds, and the preliminary observation is in agreement with the prominence of a $\pi-\pi^*$ nature of transition to the excited states[30,33] rather than $n-\pi^*$. Considering the 2-(imidazol-2-yl)phenol nucleus as the fundamental skeleton of the chromophores, absorption data shows that conjugation of the π system was extended by a methoxy substituent para to the hydroxyl group or by the fused aromatic phenanthrene group on the 4,5 positions of the imidazole ring, leading to bathochromic shifts (≈24 nm) and hyperchromism (**L1** versus **L4** and **L7**; Table 7). All ligands generally presented a red shift on coordination to zinc, except in **Z7**, which was mainly unaffected. Zinc complexes did not seem to follow a definite trend on the basis of solvent or substituent effects. In the solid thin films, the ligands generally maintained similar absorption spectral positions to those of the solution except for the *t*-Bu substituted ligands (**L6** and **L7**), which were significantly red-shifted. Apart from highlighting the role of the phenol ring in the transitions, this observation suggests that extensive interactions exist in solution similar to observed intermolecular interactions in the analyzed solid-state structures and also reveal the vibronic nature of *t*-Bu substituted **L6** and **L7**, since lesser vibration in the solid state probably enabled stronger hyperconjugation.

Ligand Fluorescent Properties. The solutions of **L1**−**L7** and **Z1**−**Z7** were prepared at the same concentration, and excitation and emission experiments were all conducted under the same spectrophotometer settings at room temperature to enable a direct comparison of spectral results. Fluorescence data and comparative overlays of emission spectra of all synthesized compounds are

(33) Park, S.; Seo, J.; Kim, S. H.; Park, S. Y. *Adv. Funct. Mater.* **2008**, *18*, 726–731.

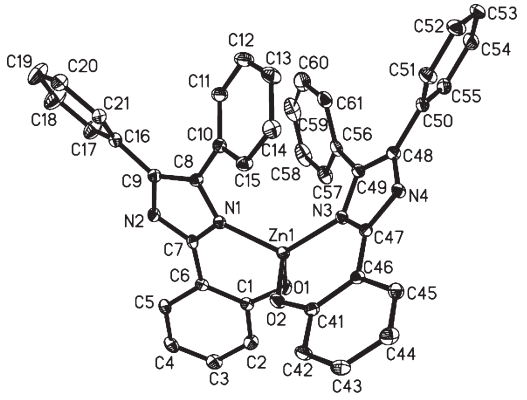

Figure 7. Molecular structure of **Z2**·$3CH_3OH$ with thermal ellipsoids drawn at the 50% probability level. Some hydrogen atoms and three methanol solvent molecules have been omitted for clarity.

Table 6. Hydrogen Bond Parameters for **Z2**·$3CH_3OH$

	D−H (Å)	D−H···A (deg)	D···A (Å)	H···A (Å)
O(5)−H(O5)···O(3)	0.782	155.32	2.711	1.981
O(4)−H(O4)···O(1)	0.757	168.49	2.679	1.933
N(2)−H(2A)···O(5)	0.879	177.88	2.855	1.976
O(3)−H(O3)···O(2)	0.778	177.40	2.701	1.923
N(4)−H(4A)···O(4)	0.880	171.58	2.870	1.997
C(5)−H(5A)···N(2)	0.951	99.65	2.916	2.602

presented in Table 8 and Figure 9a−f, respectively. In Figure 9, spectral traces of ligands and their corresponding zinc complexes in the same solvent have been plotted on identical coordinates to show changes in spectral intensities (I) of ligands in relation to the chelated analogues. In THF and methanol, an additional near-infrared emission band was observed around 800 nm for **L1** and **L2**, which was enhanced and blue-shifted on coordination to zinc in **Z1** and **Z2**. Luminescence lifetimes at all emission bands indicate a singlet excited state nature rather than a triplet one.

In general, the fluorescence lifetimes of the ligands **L1**−**L7** are longer coupled with higher-emission intensities than the respective zinc chelates. For **L1**, **L2**, **Z1**, and **Z2**, which possess two emission bands, the fluorescence lifetime monitored for both emission bands revealed similar lifetime values. **L1**, which is considered to best represent the parent 2-(imidazole-2-yl)phenol fluorophores nucleus of the series except for the 4,5-diethyl substitution, exhibited the strongest emission intensity with a quantum yield as high as 0.57 in DMF. The narrow blue emission of **L1** is also notable, with a width at half-maximum (fwhm) of 2818−2870 cm^{-1} in all solvents. The presence of substituents on the basic 2-(imidazole-2-yl)phenol framework only leads to a decrease of fluorescence quantum yields, with substituents on the phenol ring being more important in deciding the extent of emission intensity reduction. Generally, **L1**, **L2**, **L3**, and **L7** exhibited higher quantum yields compared to **L4**, **L5**, and **L6**. Relative to **L1**, the spectra of ligands in THF (Figure 9a; Table 8) show a gradual decrease in photoluminescence properties coupled with an increasing peak width for **L2** (4,5-diphenyl-substituted; fwhm = 3058 cm^{-1}) and **L7** (phenanthro-substituted with two *t*-Bu added to the phenol ring; fwhm = 2978 cm^{-1}). Similar trends were observed in methanol and DMF solutions, except that the **L7** emission

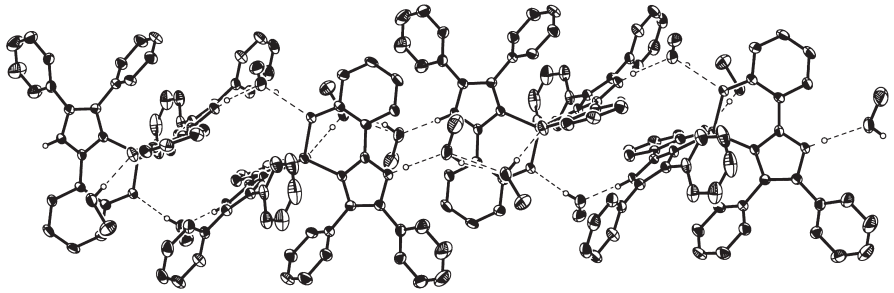

Figure 8. 1D network formed by **Z2**·3CH_3OH via H-bonding.

Table 7. Absorption Properties of **L1**−**L7** and **Z1**-**Z7**

media	ligands	$\lambda_{abs\text{-}max}$ (nm)	$\varepsilon_{(\lambda max)}$ ($M^{-1}.cm^{-1}$)	complexes	$\lambda_{abs\text{-}max}$ (nm)	$\varepsilon_{(\lambda max)}$ ($M^{-1}.cm^{-1}$)
THF	**L1**	313	15120	**Z1**	342	23080
MeOH		311	18320		329	22460
DMF		326	15360		341	25740
solid		331			329	
THF	**L2**	320	29420	**Z2**	350	28000
MeOH		316	29680		336	37840
DMF		321	18580		346	31940
solid		322				
THF	**L3**	318	43400	**Z3**	343	44120
MeOH		316	26720		331	46840
DMF		320	22580		341	42200
solid		323			338	
THF	**L4**	**337**	22240	**Z4**	338	37450
MeOH		**335**	21160		359	27720
DMF		**337**	19080		372	25160
solid		337				
THF	**L5**	325	27680	**Z5**	326	31080
MeOH		323	25340		343	26100
DMF		326	23000		345	25280
solid		327			332	
THF	**L6**	322	30840	**Z6**	323	39260
MeOH		322	23020		336	29220
DMF		322	23280		339	26040
solid		343			341	
THF	**L7**	**337**	28200	**Z7**	338	35620
MeOH		**335**	28600		335	37520
DMF		**336**	27180		336	23000
solid		**381**			371	

intensity became slightly higher than that for **L2** (Figure 9c and e). Rate constants for radiative (k_r) and nonradiative (k_{nr}) processes were calculated and are presented in Table 8. It is interesting to observe that the pendant diphenyl substituents on the 4- and 5-imidazolyl positions of **L2**−**L6** obviously caused larger nonradiative decay rate constants at the expense of the radiative decay rates (Table 8; k_r and k_{nr}; **L2**−**L6** versus **L1**, **L7** and **Z2**−**Z6** versus **Z1** and **Z7**). This is attributable to vibrational effects. Substitution of the methoxyl group at the *m* position to the phenolic OH group for **L3** caused a reduction of nonradiative decay rates relative to **L4** with the methoxy group in the *p* position. Generally, the complexes showed relatively larger k_{nr} values than the free ligands, which probably reflect a stronger vibronic nature for the excited state of the complexes. Solvent environments did not seem to produce a definite trend in affecting k_r and k_{nr} values.

Emission intensities decreased greatly for **L4**, **L5**, and **L6** in the three solvents and were mainly red-shifted relative to **L1**. However, **L3** has a moderate emission at almost the same position as **L1** in THF and MeOH, or even blue-shifted in DMF. Regarding the general red shift with respect to **L1**, some form of extension of conjugation by the various substituents could be concluded. Therefore, the effect of substituents on reducing emission capacity could be attributed to vibrational quenching or a loss of conjugation between imidazole and phenol rings through a loss of coplanarity, especially in the cases bearing the bulky phenyl or *t*-Bu substituents (Figure 9a, c, and e). This is also supported by the relatively larger ellipsoids observed in the solid state for the distal phenyl ring carbons of coordinated **L2** (C18, C19; Figure 7). A more extensive conjugated system is formed by virtue of the phenanthrene group in **L7**, which is evidenced by a consistently large spectral red shift. **L7** is thus electronically robust and different in the series. Consequently, spectral parameters for **L7** are largely unperturbed in different solvents, unlike for **L1**−**L6** (Table 8 and Figure 9:a, c, and e).

On the basis of the **L2** molecular framework, **L3**−**L6** molecular structures are only different by substituents R^2, R^3, and R^4 (Scheme 2). These substituents all caused the quantum yield to decrease greatly (Table 8), especially with R^2 and R^4 having greater influence. The alkyl or −OMe groups can lead to some extent of loss of coplanarity between the five-membered imidazole ring and

Table 8. Solution and Solid Emission Data for **L1**−**L7** and Their Zinc Complexes (**Z1**−**Z7**)

	Ligands								Zinc complexes							
Media		λ_{maxEm} (nm)	λ_{maxEx} (nm)	$\Delta\lambda^a$ (nm)	τ (ns)	Φ_F	$k_r \times 10^8$ (S^{-1})	$k_{nr} \times 10^8$ (S^{-1})		λ_{maxEm} (nm)	λ_{maxEx} (nm)	$\Delta\lambda^a$ (nm)	τ(ns)	Φ_F	$k_r \times 10^8$ (S^{-1})	$k_{nr} \times 10^8$ (S^{-1})
THF	**L1**	434[b]	325	109	4.0	0.45	1.125	1.375	**Z1**	387[b]	364	23	3.9	0.19	0.487	2.077
MeOH		**353, 416**[b]	324	**29, 92**	3.3	0.57	1.727	1.303		378[b]	328	50	2.4	0.19	0.792	3.375
DMF		427	320	107	4.2	0.56	1.333	1.048		386	363	23	1.0	0.26	2.600	6.634
solid		418	327	91						415	353	62				
THF	**L2**	449[b]	344	105	2.4	0.26	1.083	3.083	**Z2**	406[b]	375	31	0.9	0.24	2.667	8.444
MeOH		430[b]	341	89	2.4	0.39	1.625	2.542		394[b]	362	32	1.0	0.22	2.200	7.800
DMF		443	340	103	2.4	0.28	1.167	3.000		402	374	28	1.0	0.20	2.000	8.000
solid		444	330	114						395	368	26				
THF	**L3**	443	348	95	2.9	0.13	0.448	3.000	**Z3**	406	374	32	1.1	0.23	2.091	7.000
MeOH		413	340	73	2.2	0.23	1.045	3.500		394	360	34	1.2	0.25	2.083	6.250
DMF		408	356	52	1.3	0.11	0.846	6.846		407	369	38	1.4	0.24	1.714	5.429
solid		422	337	85						415	366	49				
THF	**L4**	**379, 500**	355	**24, 145**	1.3	0.06	0.462	7.231	**Z4**	441	384	57	1.1	0.08	0.727	8.364
MeOH		**373, 467**	339	**34, 128**	1.0	0.13	1.300	8.700		428	388	40	1.1	0.12	1.091	8.000
DMF		443	371	72	1.3	0.03	0.231	7.462		440	397	43	1.3	0.17	1.308	6.385
solid		486	337	**149**						421	372	49				
THF	**L5**	471	348	123	2.3	0.08	0.348	4.000	**Z5**	421	373	48	2.0	0.15	0.750	4.250
MeOH		452	346	106	1.2	0.05	0.417	7.917		418	371	47	0.8	0.09	1.125	11.375
DMF		420	365	55	0.8	0.01	0.125	12.375		421	382	39	0.9	0.12	1.333	9.777
solid		465	343	122						417	375	42				
THF	**L6**	469	349	120	2.5	0.07	0.280	3.720	**Z6**	419	367	52	2.3	0.09	0.391	3.957
MeOH		456	343	113	1.3	0.07	0.538	7.154		423	373	50	0.9	0.15	1.667	9.444
DMF		422	361	61	1.1	0.01	0.090	9.000		421	377	44	0.9	0.15	1.667	9.444
solid		474	342	132						443	410	33				
THF	**L7**	483	361	122	2.9	0.34	1.172	2.276	**Z7**	432, 466	378	54, 88	2.9	0.15	0.517	2.931
MeOH		471	359	112	1.9	0.25	1.316	3.947		468	372	96	1.9	0.27	1.421	3.842
DMF		484	369	115	3.1	0.35	1.129	2.097		482	372	110	3.1	0.29	0.935	2.290
solid		481	377	104						448	386	62				

[a] $\Delta\lambda$ = Stokes shift [b] Additional emission was observed around 800 nm.

phenol ring, which results in a weaker fluorescence. For instance, the X-ray structure of **L1** showed an imidazole−phenol plane tilt of 3.36° (between plane of C35−C34−C33−N5−N6 and plane C27−C32−C28−C29−C31−C30); meanwhile, 5.86° (between N1−N2−C7−C8−C9 and C1−C2−C3−C4−C5−C6) was observed for **L5** with a dimethyl substituent. The drastic and progressive lowering of the emissive property in going from **L2** (R^2 = R^3 = R^4 = H) to **L5** (R^2 = R^4 = Me; R^3 = H) and **L6** (R^2 = R^4 = *t*-Bu) (Figure 9a, c, and e) could be attributed to the role of vibrational deactivation and the importance of the phenol ring in the electronic transitions.

Although both **L3** and **L4** bear the methoxyl group on the phenol ring, the substituent effects differ due to the substituent position. Particularly, it is noteworthy that a methoxyl substituent at the para position from a hydroxyl group in **L4** resulted in a significant decrease in radiative relaxation in all solvents compared to that in **L2** and in contrast to the case for **L3** with the same substituent at the meta position.

The spectra of **L1** in methanol and those of **L4** in methanol and THF (Figure 10a, b) show emission bands that significantly overlapped with the respective longer-wavelength excitation bands (Stokes shifts within 27−34 nm; Table 8). Therefore, photorelaxation for **L1** and **L4** in the mentioned media gave emissions originating from both the primary enol excited state and the excited state tautomer. It could be concluded that phototautomerization is, to some extent, hindered in the affected systems. The rapid and total conversion of the excited state enol form into the excited state keto tautomer, which has hitherto been concluded by kinetic,[11] theoretical,[21,30,34] and previous experimental findings,[12,20−30,33−35] was not strictly followed in the current work. Emission bands for **L4** with a Stokes shift showed a value of 72 nm in DMF, 145 nm in MeOH, and 128 nm in THF belonging to ESIPT emissions. The lower Stokes shift bands appeared alongside the ESIPT bands in THF and MeOH, which corresponds to a significant primary photorelaxation for **L4** in THF and MeOH (Table 8). Therefore, one obvious factor responsible for this unusual phenomenon is a reduction in overlap between energies of excited enol configuration and the excited keto tautomer configuration (Scheme 4). The effect of solvent in affecting the transformation of excited state configurations in the concerned solutions is such that conversion to the keto tautomer is less favored. A potential barrier to intramolecular proton transfer of the ligands is due to intermolecular hydrogen bonding or proton transfer between the ligand and solvent (e.g., between the imidazole nitrogen base and methanol proton or between THF and the phenolic proton). However, the exact role of the solvent is not yet clear. Measurements of fluorescence lifetime gave undistinguishable values at both excited enol and excited keto tautomer emissions, which suggests that the relaxation process depends on the population of enol tautomer and supports a conclusion about a delayed ESIPT process. Solid-state emission positions for the

(34) Zheng, S.-L.; Zhang, J.-P.; Chen, X.-M.; Huang, Z.-L.; Lin, Z.-Y.; Wong, W.-T. *Chem.—Eur. J.* **2003**, *9*, 3888–3896.

(35) Park, S.; Kwon, O.-H.; Kim, S.; Park, S.; Choi, M.-G.; Cha, M.; Park, S. Y.; Jang, D.-J. *J. Am. Chem. Soc.* **2005**, *127*, 10070–10074.

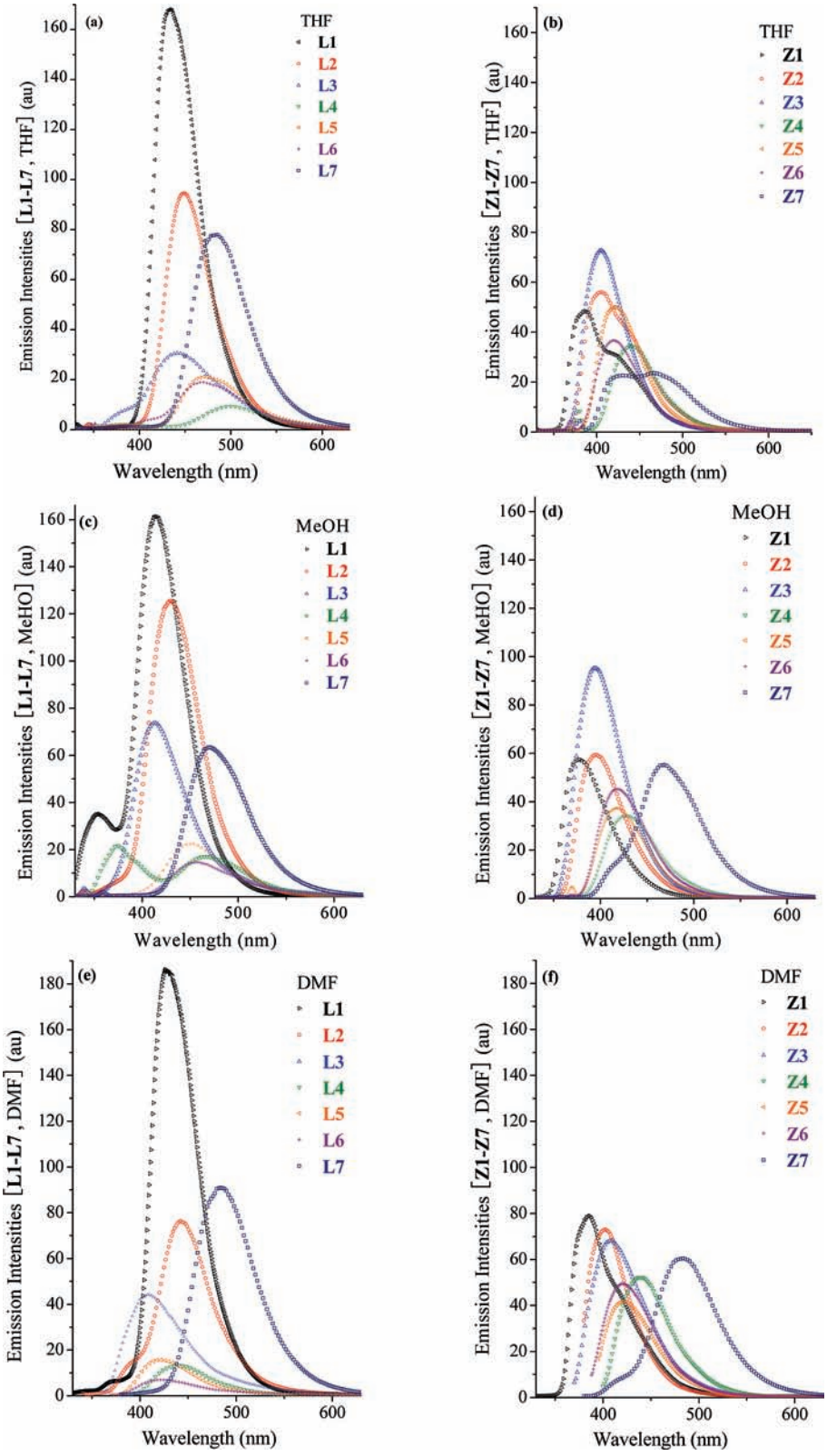

Figure 9. Relative emission intensities of ligands **L1**−**L7** and their corresponding complexes **Z1**−**Z7** in THF (a and b), MeOH (**c** and **d**), and DMF (**e** and **f**) solutions, respectively.

ligands are generally within the values observed in their solutions. This suggests a dominance of the extensive hydrogen bonding interactions over stacking.

Fluorescent Properties of Zinc Complexes. The spectral overlay of the neutral zinc complexes in THF, methanol, and DMF are shown in Figure 9b, d, and f, respectively. All emissions occur with significant blue shifts relative to corresponding ligands. In order to rationalize the factors responsible for the blue-shifted fluorescence spectra of complexes, electronic perturbation of the chelated ligands

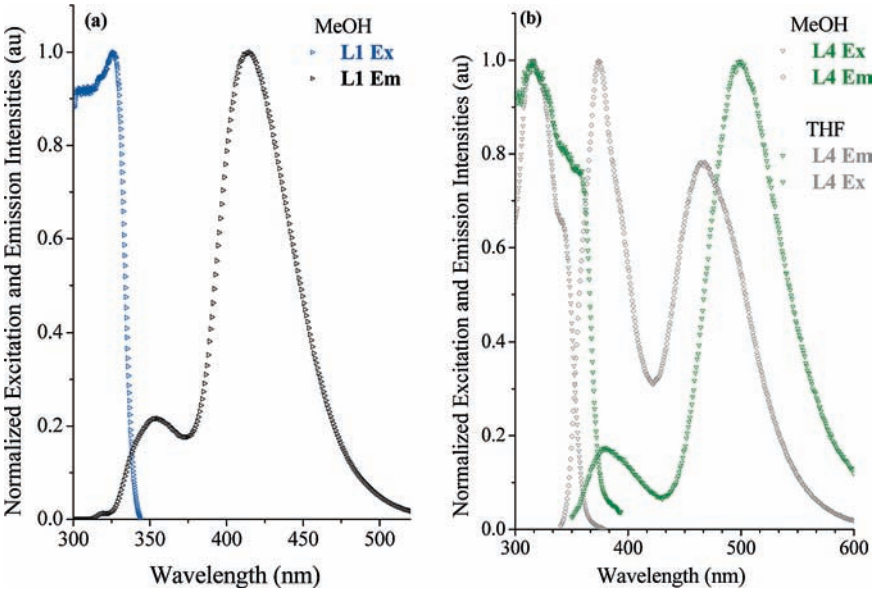

Figure 10. Normalized excitation and emission spectra showing overlap of primary emission bands with excitation spectra for (a) **L1** and (b) **L4**.

Scheme 4. Schematic Representation of the Unusual Photocycle Observed for **L1** and **L4**

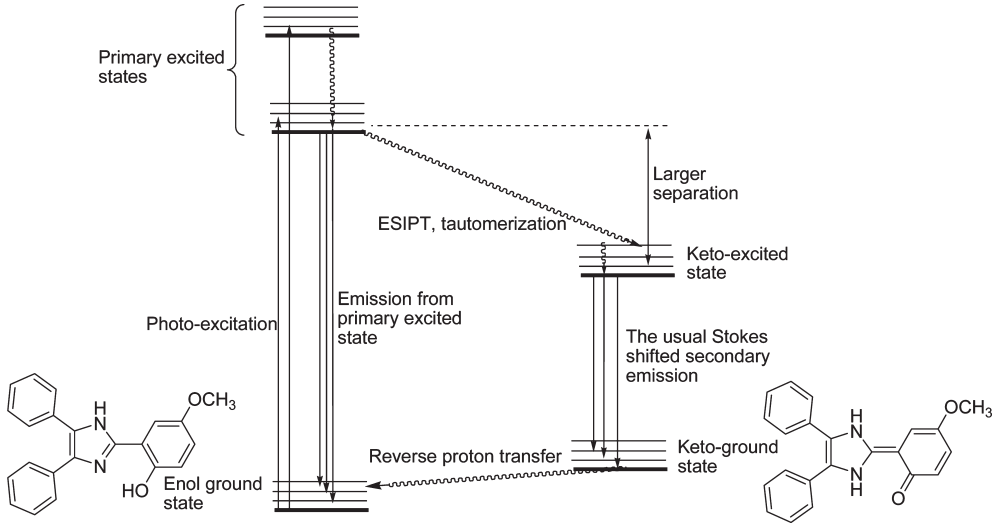

can be mentioned. On ligand coordination with Zn^{2+}, net valence transfer is from the ligand to the zinc ion. Due to the transfer of frontier orbital electrons toward the Zn^{2+} ion orbital, all local frontier π-orbital energies are lower, and both the absorption and the emission spectrum bands should undergo a blue shift. The overlap of excitation and emission spectral bands coupled with a corresponding lower Stokes shift both support a loss of phototautomerization possibilities due to the absence of a phenolic proton (Figure 11, Table 8).[36]

In the series, fluorescence intensities of chelated ligands can be classified as enhanced (**Z3**, **Z4**, **Z5**, and **Z6**) or quenched (**Z1**, **Z2**, and **Z7**) with respect to those of free ligands. Such an observation is contrary to some zinc complexes reported to consistently intensify,[37−39] quench,[40] or maintain no influence[21,36] on the fluorescence of ligands after chelation. Generally, the emission intensity of **Z3** was observed to be higher than that of other complexes. It is probable that the methoxy group has the capacity to compensate for the valence electron transfer of the ligand π orbital to the zinc ion when located on the meta position relative to the oxo atom. It is observable that each case of quenching after coordination was accompanied by a significant blue shift of the emission band (e.g., **L1**, **L2**, and **L7**; Figure 12a), while the cases involving enhancement show emission peaks at roughly the same positions as the free ligands (e.g., **L4**, **L5**, and **L6**; Figure 12b).

(36) Görner, H.; Khanra, S.; Weyhermüller, T.; Chaudhuri, P. *J. Phys. Chem. A*. **2006**, *110*, 2587–2594.
(37) Huston, M. E.; Haider, K. W.; Czarnik, A. W. *J. Am. Chem. Soc.* **1988**, *110*, 4460–4462.
(38) Koike, T.; Abe, T.; Takahashi, M; Ohtani, K.; Kimura, E.; Shirob, M. *J. Chem. Soc., Dalton Trans*. **2002**, *2002*, 1764–1768.
(39) Ruf, M.; Durfee, W. S.; Pierpont, C. G. *Chem Commun*. **2004**, *2004*, 1022–1023.
(40) Sohna, J.-E. S.; Jaumier, P.; Fages, F. *J. Chem. Res. (S)*. **1999**, *1999*, 134–135.

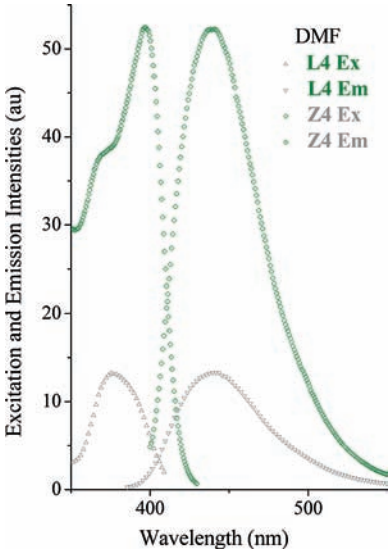

Figure 11. Excitation and emission spectra of **L4** and **Z4** in DMF.

Considering solvent effects, methanol has almost no significant influence relative to THF solvent except for a shortening of lifetimes to some extent for **L1**−**L6**. No regular difference could be observed between solution and solid emission properties of the zinc complex series.

Fluorescent Response of L2 and L4 under Zn^{2+} Titration. In an effort to explore the potential of this ligand system as zinc sensors, emission scans were performed on 1×10^{-4} M solutions of **L2** (in MeOH) and **L4** (in DMF) in the presence of $0-5 \times 10^{-8}$ M zinc(II) ions. The representative ligands studied were selected on the basis of quenching (**L2**) and enhancing (**L4**) behaviors resulting from coordination to Zn^{2+}. It was observed that the emission intensities displayed a significant and linear response to the presence of Zn^{2+} even at Zn^{2+}/ligand molar ratios as low as 1:10 000 to 5:10 000. These findings suggest the applicability of the ligand systems for the quantitative estimation of free Zn^{2+} in water miscible solvents such as methanol and DMF.

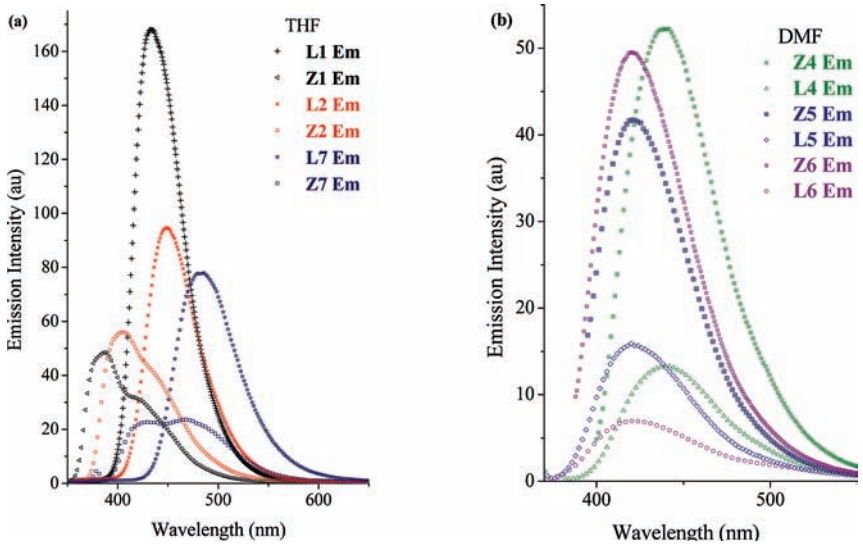

Figure 12. (a) Quenching of **L1**, **L2**, and **L7**; (b) enhancement of **L4**, **L5**, and **L6**.

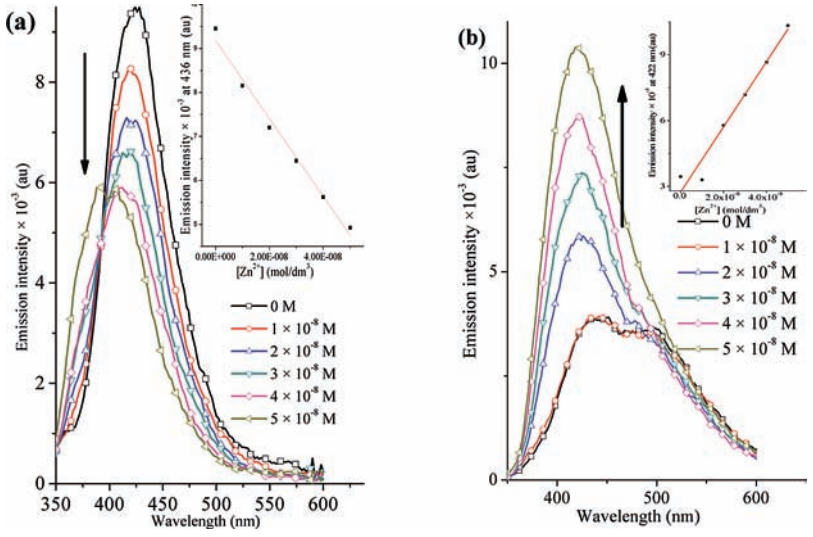

Figure 13. Fluorescence response on Zn^{2+} titration ($0-5 \times 10^{-8}$ M) for **L2** (a) and **L4** (b).

Conclusions

A series of 2-(imidazole-2-yl)phenol ligands, **L1**−**L7**, and their bis-chelate Zn(II) complexes (**Z1**−**Z7**) were prepared and characterized. Structures of **L1**, **L5**, **Z1**, and **Z2** were confirmed by single-crystal X-ray diffraction experiments. One-dimensional arrays based on continuous $\pi-\pi$ stacking interactions and hydrogen bonding were observed in the solid states of **L1**, **L5**, and **Z1**. **Z2** also adopted hydrogen-bonding 1D networks without $\pi-\pi$ stacking interactions. Photoluminescence properties of the ligands and complexes were studied and comparatively discussed on the basis of experimentally observed substituent and condensed media effects. The presence of substituents on the 2-(imidazole-2-yl)phenol skeleton only leads to a reduction in radiative relaxation properties, and substituents on the phenol ring are more relevant for controlling emission properties of the basic skeleton. **L1** should be a potential candidate for organic emitting applications based on high fluorescence intensities in solid film and solutions. In contrast to the general conclusions on the ESIPT photoprocess for phenols bearing a base as the ortho substituent, significant photorelaxation from excited enol states was observed for **L1** in methanol and for **L4** in both THF and methanol. Therefore, we can conclude that there exists a certain unusual hindering factor to enol−keto phototautomerism and that substituents as well as condensed media play important roles in luminescence processes of the family of ligands. The coordination of zinc with ligands (**L1**−**L7**) caused enhancement or quenching effects of intensities of fluorescence relative to free ligands. Electron-rich substituents such as the methoxyl group were found to be suitable for ensuring better emission intensity in the zinc complexes. The linear quenching or enhancement of fluorescence observed in the presence of Zn^{2+} at 10^{-8} M orders of concentration and Zn^{2+}/ligand molar ratios of 1:10 000 indicates applicability of these ligand systems for the quantitative analytical estimation of free Zn^{2+} samples in water miscible solvents.

Acknowledgment. The authors thank the National Natural Science Foundation of China for support of this research (Grant No. 20773149). A.O.E. is grateful to the Chinese Academy of Science (CAS) and the Academy of Science for The Developing World (TWAS) for the Postgraduate Fellowships and Redeeme's University for study leave. Prof. Dr. Joshua A. Obaleye (Department of Chemistry, University of Ilorin, Ilorin Kwara state, Nigeria) is thanked for his kind proofreading of the manuscript.

Supporting Information Available: Crystallographic details for all structures in the form of CIF files and solid-state photoluminescence spectra. This material is available free of charge via the Internet at http://pubs.acs.org.